




Structural evaluation of ZnO substitution for CaO in glass ionomer cement synthesized by sol-gel method and their properties

Oranich Thongsri¹, Sawitri Srisuwan¹, Paritat Thaitalay¹, Rawee Dangwiryakul¹, Prasert Aengchuan², Narong Chanlek³, Pinit Kidkhunthod³, Chutima Talabnin⁴, Sanong Suksaweang⁵, and Sirirat Tubsungnoen Rattanachan^{1,*} 

¹ School of Ceramic Engineering, Institute of Engineering, Suranaree University of Technology, Nakhon Ratchasima, Thailand

² School of Manufacturing Engineering, Institute of Engineering, Suranaree University of Technology, Nakhon Ratchasima, Thailand

³ Synchrotron Light Research Institute (Public Organization), Nakhon Ratchasima, Thailand

⁴ School of Biochemistry, Institute of Science, Suranaree University of Technology, Nakhon Ratchasima, Thailand

⁵ School of Pathology and Laboratory Medicine, Institute of Medicine, Suranaree University of Technology, Nakhon Ratchasima, Thailand

Received: 13 June 2021

Accepted: 7 September 2021

Published online:
3 January 2022

© The Author(s), under exclusive licence to Springer Science+Business Media, LLC, part of Springer Nature 2021

ABSTRACT

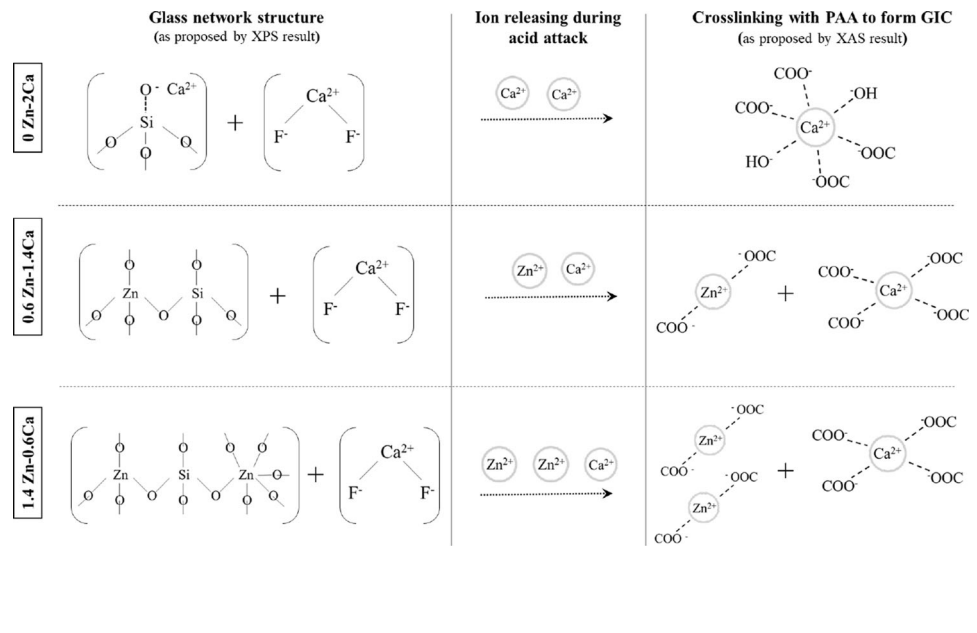
The substitution of ZnO for CaO site and the limitation of ZnO addition in the sol-gel ionomer glass composition at different calcination temperatures were evaluated and characterized in-depth by X-ray powder diffraction and X-ray photoelectron spectroscopy techniques in this study. The relationship between the compressive strength and the final cement structure was demonstrated by the ion-releasing behavior and synchrotron-based X-ray absorption spectroscopy (XAS) technique. The setting time, in vitro cytotoxicity, bioactivity and tooth adhesion ability of the sol-gel GICs were also evaluated. As expected, ZnO containing GICs presented antibacterial properties under the visible light condition as photocatalysis effect. Although the low crosslinking ability of Zn atoms to the polyacrylic liquid reduced the compressive strength, the compressive strength could be improved by compromising the calcination temperature. Moreover, this study also shows that the ZnO containing GICs had promising results on the biological properties which offered potential advantages in clinical use.

Handling Editor: David Cann.

Address correspondence to E-mail: sirirat.b@g.sut.ac.th

<https://doi.org/10.1007/s10853-021-06517-6>

GRAPHICAL ABSTRACT



Introduction

Dental caries is the leading oral health problem which mainly caused by acid-produced bacteria resulting in subsurface demineralization of the teeth [1]. The main treatment option when caries have progressed is filling with a dental restorative material.

The conventional glass ionomer cement (GIC) is attractive for dental restoration because it can release fluoride ions into the oral cavity leading to tooth decay resistivity [2]. This material is made of acid-base reactions of two compositions which were polyacrylic acid and ion-leachable glass based on aluminosilicate glass composed of fluoride and various metal oxide i.e., CaO, SrO, NaO, P₂O₅, etc. [3].

Zn²⁺ ions are known as a bactericidal agent inhibiting the formation of caries [4, 5]. The incorporation of zinc in GIC was reported several benefits, including enhancement of flexural strength, surface roughness, good abrasive wear [6, 7]. Additionally, it was known that Ca²⁺ ions (or Sr²⁺ ion) played important role in the glass network structure as a charge balancing agent and the GIC structure as a crosslinking ion [3, 8]. Since Zn²⁺ ions have the same charge as Ca²⁺ ions, Zn²⁺ ions were supposed to act

as a replacement for Ca²⁺ ions. However, there was literature reporting that the incorporation of zinc in the aluminosilicate glass which derived by traditional melt-quenching process increased a glass structural density and induced some crystallization [9]. The traditional melt-quenching preparation of the glass ionomer is carried out at 1,300–1,500 °C [10]. This temperature range could result in fluoride loss during melting and uncontrollable glass composition [11].

The sol-gel process becomes an attractive option for glass synthesis. This process is based on the hydrolysis and condensation reaction; hence, it is possible to prepare homogeneous, high-temperature glasses at low temperature (600–800 °C), with the controllable doping content at a molecular level [12, 13]. Although the sol-gel technique has numerous benefits, it is sensitive to the synthesis conditions especially the thermal history of the process that influence the final product structure which should be investigated [11, 13–15]. Moreover, there was a lack of literature reporting the effect of ZnO contents instead of CaO in GIC synthesized by the sol-gel method on the relationship of the glass network structure, the GIC structure and their properties.

In this study, we aimed to investigate the effect of ZnO doping instead of CaO in the ionomer glass

composition and the calcination temperature on the sol-gel glass structure affecting the compressive strength and antibacterial property under dark condition and visible light. The chemical structure of the ionomer glasses and the GICs were in-depth analyzed by XPS and XAS characterization techniques to evaluate ZnO substitution in CaO of the sol-gel glass structure. To understand the setting reaction and the limit of ZnO content in the ionomer glass composition, the ion-releasing behavior of the sol-gel ionomer was investigated. Additionally, cytotoxicity, bioactivity and adhesion to the tooth surface for this sol-gel GIC were evaluated as well.

Material and method

Preparation of ionomer glass

The ionomer glass was synthesized by the sol-gel method using an analytical grade of tetraethyl orthosilicate (TEOS, 98%, Acros), aluminum nitrate ($\text{Al}(\text{NO}_3)_3$, 98%, Ajax), triethyl phosphate (TEP, 99%, Acros), calcium nitrate tetrahydrate ($\text{Ca}(\text{NO}_3)_2 \cdot 4\text{H}_2\text{O}$, Ajax), hydrofluoric acid (H_2SiF_6 , Acros), and absolute ethanol (EtOH, Carlo Erba) as the chemical precursors.

The synthesis process in this experiment was adapted from the previous work [8]. Briefly, the synthesis process started by adding TEOS into the mixed solution of DI water and EtOH. Next, $\text{Al}(\text{NO}_3)_3$, TEP and $\text{Ca}(\text{NO}_3)_2$ were sequentially added and stirred by a magnetic stirrer. Then, the solution was aged under an acid condition at a temperature in a range of 80–85 °C, and the gel was dried at 100 °C. The dried gel was calcined at 600–750 °C, then ground in a planetary mill to obtain the fine glass powder.

Design of experiment (DOE)

DOE technique was used for the preliminary study in order to survey the significant factor and design the further experiment [16]. The 2 k full factorial was designed by Minitab 16 statistical software to determine the effect of ZnO substitution for CaO in the ionomer glass on the compressive strength of the sol-gel GICs. The ionomer glass compositions in this experiment were designed as presented in Table 1. Moreover, the calcination temperatures for gel-

Table 1 Design composition for the sol-gel ionomer glass

Sample code	Mol ratio					
	Si	Al	P	F	Ca	Zn
0Zn	4.5	4	0.16	4	2	0
0.6Zn					1.4	0.6
1.0Zn					1	1
1.4Zn					0.6	1.4

derived glass at 650 °C and 750 °C were also studied in this work.

Characterization of the sol-gel glass for glass ionomer cement

The chemical structure of the sol-gel glass was analyzed by a German Bruker D2 X-ray diffractometer (XRD) with a step time of 0.02°/min and a scan range of 10–60°. X-ray photoelectron spectroscopy (XPS) technique was used to characterize the glass network structure of the sol-gel ionomer glass. The measurement was performed using PHI5000 Versa Probe II, ULVAC-PHI, Japan, at the SUT-NANOTEC-SLRI joint research facility, Synchrotron Light Research Institute (SLRI), Thailand. The monochromatic Al K-alpha radiation (1486.6 eV) was used as an excitation source. The C1s peak of carbon at 284.8 eV binding energy was used to calibrate the binding energies. The fitting curves of XPS spectra were processed by PHI MultiPak XPS software using a combination of Gaussian-Lorentzian lines.

In this study, ion-releasing concentrations of the sol-gel glass powders were evaluated to determine the ions that affected the setting reaction in GIC. Thus, the ion-releasing behavior of the ionomer glass was conducted in acetic acid. The sol-gel ionomer glass was soaked in 5% acetic acid for 2, 6, 10, and 60 min, respectively. The concentrations of ions (Si, Al, P, Ca and Zn) released from the ionomer glass were measured by the Inductively Coupled Plasma (ICP-OES optima 8000, Perkin).

After the setting reaction, the GIC specimens were evaluated by the synchrotron-based X-ray absorption spectroscopy (XAS) technique including in-situ X-ray absorption near edge structure (in-situ XANES) and in-situ extended X-ray absorption fine structure (in-situ EXAFS) in order to analyze local structural information around Ca and Zn atoms. The

measurement was conducted at the SUT-NANOTEC-SLRI XAS Beamline (BL5.2) at the Synchrotron Light Research Institute (Public Organization), Thailand [17]. The data were analyzed and fitted by Athena and Artemis program as implemented in the IFEFFIT packages [18]. The reference standard curves were from the material project (file number; mp-2605_CaO and mp-1986_ZnO) [19].

GIC sample preparation and testing

The liquid solution for GIC preparation was the mixture of the polyacrylic acid (35 wt.% in H₂O PAA; MW ~ 100,000) and tartaric acid in the ratio of 9:1 w/w supplied by Sigma-Aldrich. The GIC samples were prepared by mixing the sol-gel glass powders with the liquid solution at a powder to liquid ratio (P/L) of 1/1 (w/v).

The net setting time of the GICs was determined by Gillmore Apparatus (Humboldt, H-3150F) following ISO 9917-1 for dental glass polyalkenoate cement. After mixing the cement paste, the paste was filled into the cylindrical Teflon mold with 10 mm in diameter and 2 mm in height. The net setting time was measured when a heavy and thin needle (453.6 g, Ø 1.06 mm) was placed on the paste surface every 5 s until no mark occurred. The testing was carried out at room temperature three times.

Compressive strength was measured according to ISO 9917-1:2007 using the universal testing machine (UTM, Instron 5565, Instron GmbH, Germany) with 5 kN load cells. The cross-head speed was 0.75 mm/min according to the previous literature [20]. The GIC specimens were prepared in the cylindrical shape Teflon mold with 4 mm in diameter and 6 mm in height. After being molded for 1 h, all the specimens were kept in DI water at 37 °C for 23 h before testing. At least eight specimens were prepared for each experimental condition. The compressive strength was calculated using the equation, $CS = 4P/\pi d^2$, where CS was compressive strength (MPa), P was the maximum load applied (N), and d was specimens radius (mm).

Antibacterial testing

The antibacterial activity of the sol-gel-derived GICs was tested against *Streptococcus mutans* (ATCC 27,145) using the agar disk diffusion method in comparison with the commercial GIC (Fuji IX extra,

GC corporation, Tokyo, Japan). The *Streptococcus mutans* was cultured at 37 °C, 5%CO₂ for 24 h. The bacteria were swabbed uniformly on the newly made Mueller-Hinton agar plate. The disk-shaped GIC samples were then placed onto the agar and incubated at 37 °C for 48 h. The antibacterial testing was subjected to both dark and visible light conditions. For a dark condition, the plates were immediately placed in the black box before putting into the incubator. For the visible light condition, the plates were processed and incubated without placing them in the black box. The inhibition zone of bacterial activities was evaluated by measuring the diameter of inhibition zones around the GIC disks. The calculation of inhibition zone size was provided as follows: size of inhibition zone (mm) = (diameter of inhibition zone – diameter of disk)/2.

Cell viability

Cytotoxicity of GICs was demonstrated by the cell viability of NIH/3T3 fibroblast after GIC extracts treatment that was evaluated by MTS assay. The GICs were molded in disk shape (Ø = 12 mm, $h = 2$ mm) and set in the air for 1 h. Consequently, the GIC disks were sterilized by UV light for 30 min on each side and rinsed by 1 × PBS. The GIC extracts were prepared by immersing the cement disks in 1 ml of the cell culture medium and incubated at 37°C for 24 h. The culture medium consisted of 44% Dulbecco's Modified Eagle Medium (DMEM (1X) from Invitrogen, USA), 44% F-12 Nutrient mixture (HAM from Invitrogen, USA), 10% Fetal Bovine Serum (FBS from Invitrogen, USA) 1% L-glutamine and 1% Penicillin streptomycin (Invitrogen, USA). The NIH/3T3 fibroblast cells were seeded at a density of 5,000 cells/well in 96 well plates. After 24 h of seeding, the cells were treated with various concentrations of the GIC extract (0, 0.6 and 1.4 ZnO) for 24 h. The cells with culture media were used as a negative control. The cell viability was tested by dropping 20 µl of MTS reagent (CellTiter 96® AQueous) into each well plate. After incubation for 2 h, the optical density was measured at 490 nm (OD490) using an automated plate reader. The percentage of viable cells was calculated from OD values using the following equation [21]: %Cell viability = (Sample absorbance value/Control group absorbance value) × 100.

Additionally, the extracted medium was also collected and diluted into 20-fold DI water to evaluate the concentration of released Zn^{2+} ions by using the ICP-OES technique (ICP-OES optima 8000, Perkin).

Ability of apatite-like formation and tooth-GIC interface

To investigate the ability of apatite-like formation on the GIC surface, the GIC doping with 0, 0.6 and 1.4 ZnO were prepared in a cylindrical shape, with 2 mm in height and 10 mm in diameter. Then, the specimens were soaked in artificial saliva for 5 days. The composition of the artificial saliva employed in this study was 0.4 g Sodium chloride (NaCl, 98%, Carlo Erba), 0.4 g Potassium chloride (KCl, 99.5%, Merck), 0.795 g Calcium chloride ($\text{CaCl}_2 \cdot \text{H}_2\text{O}$, Merck), 0.69 g Sodium phosphate monobasic monohydrate ($\text{NaH}_2\text{PO}_4 \cdot \text{H}_2\text{O}$, 98%, Merck), 0.005 g Sodium sulfide nonahydrate ($\text{Na}_2\text{S} \cdot 9\text{H}_2\text{O}$, 98%, Carlo Erba) and 1000 mL DI water [22].

In order to observe the tooth-GIC interface, the premolar teeth were drilled and filled with the GIC doping with 0, 0.6 and 1.4 ZnO. After leaving in the air for 1 h, all specimens were transferred to the artificial saliva and incubated at 37 °C for 7 days. Consequently, the specimens were mounted in the resin following by cutting a cross-section to observe the interfacial area between the tooth and the GIC. The surface morphology of both bioactivity and tooth adhesive specimens were observed by scanning electron microscope (SEM, JEOL-6010LV) at an acceleration voltage of 15 kV. All specimens were coated with gold before the examination.

Result and discussion

Characterization of the sol-gel-derived ionomer glass

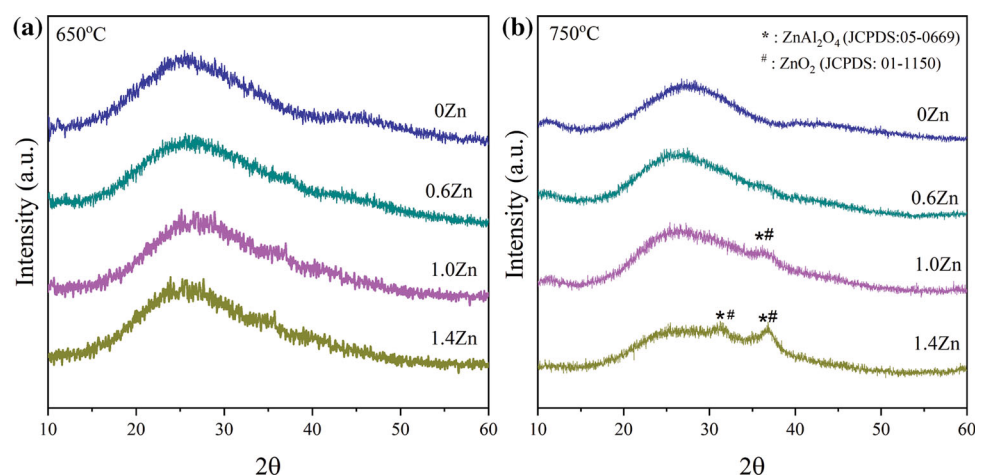
Figure 1 presents XRD patterns of $4.5\text{SiO}_2\text{-}4\text{Al}_2\text{O}_3\text{-}0.16\text{P}_2\text{O}_5\text{-}(2\text{-}x)\text{Ca-xZnO-}2\text{F}_2$, where $x = 0, 0.6, 1.0$ and 1.4 , synthesized by the sol-gel method at the different calcination temperatures. All XRD patterns show the amorphous phase. However, 1.4 mol doped ZnO sol-gel glass calcined at 750 °C revealed a peak around 2θ of 38, attributing to the formation of the crystal ZnAl_2O_4 (JCPDS:05-0669) and ZnO (JCDPS:01-1150) phase. The crystallinity of the glass increased with increasing the calcination temperature, as shown in Fig. 1b.

In general, the sol-gel process, colloidal suspension or sol is formed by hydrolysis of the starting composition. The liquid sol then transforms to be a wet gel during polymerization. Finally, the wet gel converts into dense ceramic by drying and heat treatment [23]. The heating step and slow cooling rate of the sol-gel process easily induced phase separation and crystal growth [14, 24]. This can be seen in Fig. 1 that the crystal structure was found when the calcination temperature was increased.

The chemical states of oxygen, aluminum and zinc for the sol-gel glasses were evaluated using the XPS technique as shown in Fig. 2. Deconvolution curves were processed by PHI MultiPak XPS software using a combination of Gaussian-Lorentzian lines with a constant value of full width at half maximum (FWHM).

As can be seen in Fig. 2a, all O1s spectra of the glass showed two deconvoluted peaks locating

Figure 1 XRD pattern of the sol-gel ionomer glass belonging to the system of $4.5\text{SiO}_2\text{-}4.0\text{Al}_2\text{O}_3\text{-}0.16\text{P}_2\text{O}_5\text{-}(2\text{-}x)\text{Ca-xZnO-}2\text{F}_2$, where $x = 0, 0.6, 1.0$ and 1.4 calcined at **a** 650 °C and **b** 750 °C.



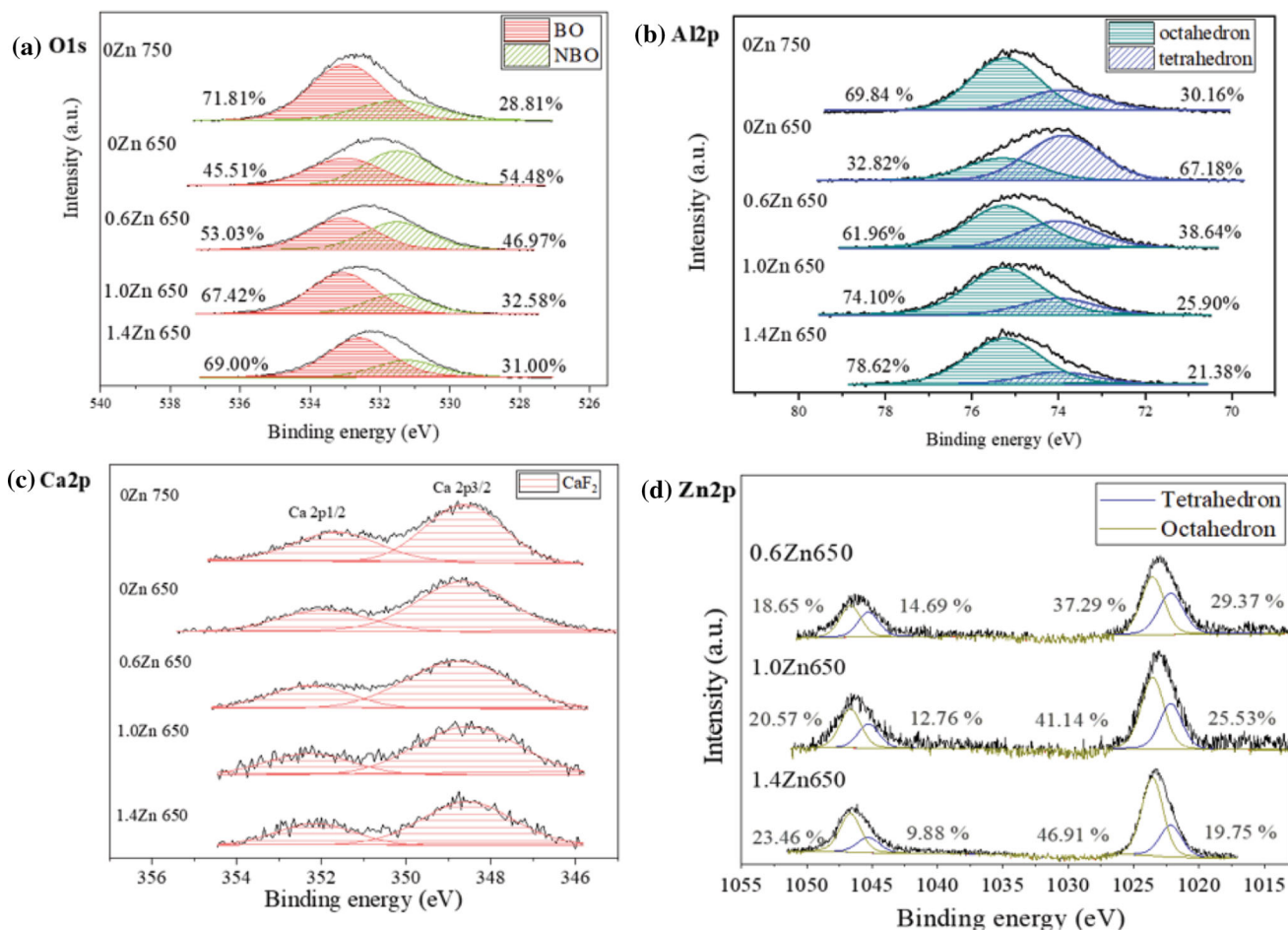


Figure 2 The high-resolution XPS spectra of **a** Oxygen (O1s) **b** Aluminum (Al2p) and **c** Zinc (Zn2p) for the sol-gel ionomer glass belonging to the system of $4.5\text{SiO}_2\text{-}4.0\text{Al}_2\text{O}_3\text{-}0.16\text{P}_2\text{O}_5\text{-}(2\text{-}$

$x)\text{Ca-xZnO-}2\text{F}_2$, where $x = 0, 0.6, 1.0$ and 1.4 calcined at $650\text{ }^\circ\text{C}$ as compared to the Zn-free ionomer glass calcined at $750\text{ }^\circ\text{C}$.

around 532.9 eV and 531.0 eV which were associated with the bridging oxygen (BO) and non-bridging oxygen (NBO) group, respectively. Without ZnO doping in the sol-gel glass, a fraction of the NBO structure was drastically decreased with the increase of the calcination temperature. Meanwhile, the fraction of NBO also decreased with the increase of ZnO doping in the glass composition.

Figure 2b presents the high-resolution XPS spectra in the Al2p region of the sol-gel glass. The deconvoluted Al2p peaks at the binding energies around 75.3 eV and 74 eV attributed to $[\text{AlO}_6]$ octahedral and $[\text{AlO}_4]$ tetrahedral structure, respectively [25]. For the Zn-free sol-gel glasses, the proportion of $[\text{AlO}_4]$ tetrahedral structure reduced with increased calcination temperature from 650 to $750\text{ }^\circ\text{C}$. As increasing Zn content in the glass composition, the $[\text{AlO}_4]$ tetrahedron was also decreased.

Figure 2c revealed the spin-orbit doublet of Ca2p with the binding energies around 348.37 and 352.02 eV . These peaks exhibited a characteristic of CaF_2 [26]. In the case of Zn-free sol-gel glass calcined at $650\text{ }^\circ\text{C}$, the peak was slightly broadened and shifted to the higher binding energy. This is attributed to the presence of Ca–O and Ca–OH bonds [27].

The Zn2p double spectra of the ZnO-doped glass is shown in Fig. 2d. The binding energies around 1045 and 1021.5 eV corresponded to tetrahedral Zn^{2+} ions, and the peaks at 1047.5 and 1024.0 eV were assigned to octahedral Zn^{2+} ions [28]. Additionally, the octahedral Zn^{2+} ions fraction increased with ZnO content in the glass composition.

XPS spectra showed the existence of Al^{3+} ions in the form of tetrahedron and octahedron. When ZnO was added to the glass composition, the $[\text{AlO}_6]$ octahedral fraction was increased. According to the

report of Kusumoto, the reason for an increase in $[\text{AlO}_6]$ octahedral species might be due to the charge balancing of Zn^{2+} ions in Al-O-PO_3^{3-} species resulting in insufficient charge balancing ion for maintaining $[\text{AlO}_4]$ tetrahedron [10]. Our finding showed the probability of ZnAl_2O_4 existence where Al^{3+} ions were in the octahedral site, and Zn^{2+} ions were in the tetrahedral site. Additionally, Zn^{2+} ions in the octahedral site were increased with ZnO content in the glass composition. It was possible that the excessive Zn^{2+} ions formed with O^{2-} ions at sixfold coordination and played a role as a charge compensation for the glass network [29].

The deconvoluted XPS spectra also presented that the increase of calcination temperature and ZnO content increased the BO fraction in the sol-gel glass structure. This structure was reported that decreased the acid susceptibility of the glass [15].

Ion-releasing behavior

The ion-releasing behavior in the acidic condition of the ionomer glasses was evaluated in order to determine the setting reaction. Figure 3 shows the ion-releasing level of the glass in the 5% acetic solutions evaluated by the ICP-OES technique. The data revealed the release of Al, Ca, Zn, Si, and P. The level of Al was exhibited in Fig. 3a. Without Zn-doped, the level of Al ions of the sample calcined at 650°C was higher than that calcined at 750°C . For the group of ZnO-doped glass, Al ions releasing level had no significant difference.

Figure 3b, c present that the ZnO addition in the glass composition caused the reduction of the releasing level of Ca ions and increased the releasing level of Zn ions along with the increase of ZnO content, respectively. In addition, the increase of calcination temperature reduced the level of calcium ions released from the glass as well.

The addition of ZnO in the glass reduced the amount of Si ions release. However, there was no significant difference in level Si ions release among the ZnO-doped series, as shown in Fig. 3d. Meanwhile, the glass calcined at 650°C released a higher level of Si ions than that of the 750°C . The ion species of Si that released to the acid solution was considered to be $\text{Si}(\text{OH})_4^{2-}$ or $(\text{SiO}_3)^{2-}$ [30].

Finally, Fig. 3e presents that all the sol-gel glasses released very small amounts of P ions and there was no significant difference among the samples. In the

case of P ions, the species that was released to the acid solution was reported to be PO_4^{3-} [31].

The initial setting reaction of the GIC was an acid-base reaction between the polymeric acid solution and the glass powder. This reaction immediately produced calcium (or strontium and zinc) polyacrylate, followed by aluminum polyacrylate slightly later. This setting took place in a period of 2–6 min. After the initial setting, it was following the secondary setting. It seemed to be that the phosphate network also played a role during the maturation reaction [32]. However, this study found no significant difference as an effect of the phosphate species. The ion species that influenced the setting reaction in this study seem to be aluminum, calcium, and zinc.

DOE analysis of the compressive strength

In order to determine the significant factor for the compressive strength of the sol-gel GICs, ZnO content in sol-gel ionomer glass and the calcination temperature were designed by the DOE technique for the primary study. This study synthesized the glass with a composition of $4.5\text{SiO}_2\text{-}4.3\text{Al}_2\text{O}_3\text{-}0.16\text{P}_2\text{O}_5\text{-}(2\text{-}x)\text{Ca-xZnO-}2\text{F}_2$, where $x = 0, 0.6, 1.0$ and 1.4 by the sol-gel method and calcined at 650°C and 750°C .

ANOVA analysis in Table 2 presents the influence of ZnO content and calcination temperature on the compressive strength of the sol-gel GICs. The statistical difference between the groups was judged to be significant when $p \leq 0.05$. This result showed that P -values of ZnO content and calcination temperature were lower than 0.05; thus, these two factors were significantly affected by the compressive strength of the sol-gel GICs. However, there was no interaction between ZnO content and the calcination temperature ($P > 0.05$) which affected the compressive strength of the cement.

Figure 4 illustrates the interaction and main effect plot for compressive strength of GIC with different ZnO contents and the calcination temperatures. Compressive strength decreased significantly where ZnO content of the glass was at $x = 0.6\text{--}1.0$, but ZnO content had not been significantly affected at $x = 1.0\text{--}1.4$. Moreover, it was found that the increasing of calcination temperature had an adverse effect on compressive strength. It should be noted that the compressive strength tended to increase when ZnO content was below 0.6 and the calcination temperature at 650°C . From these results, therefore, the effect

Figure 3 Concentration of a Al, b Ca/Sr, c Zn, d Si and e P ions releasing from the sol-gel ionomer glass belonging to the system of $4.5\text{SiO}_2-4.0\text{Al}_2\text{O}_3-0.16\text{P}_2\text{O}_5-(2-x)\text{Ca}-x\text{ZnO}-2\text{F}_2$, where $X = 0, 0.6, 1.0$ and 1.4 calcination temperature of 650°C in comparison to Zn-free ionomer glass calcined at 750°C as a function of the immersion time.

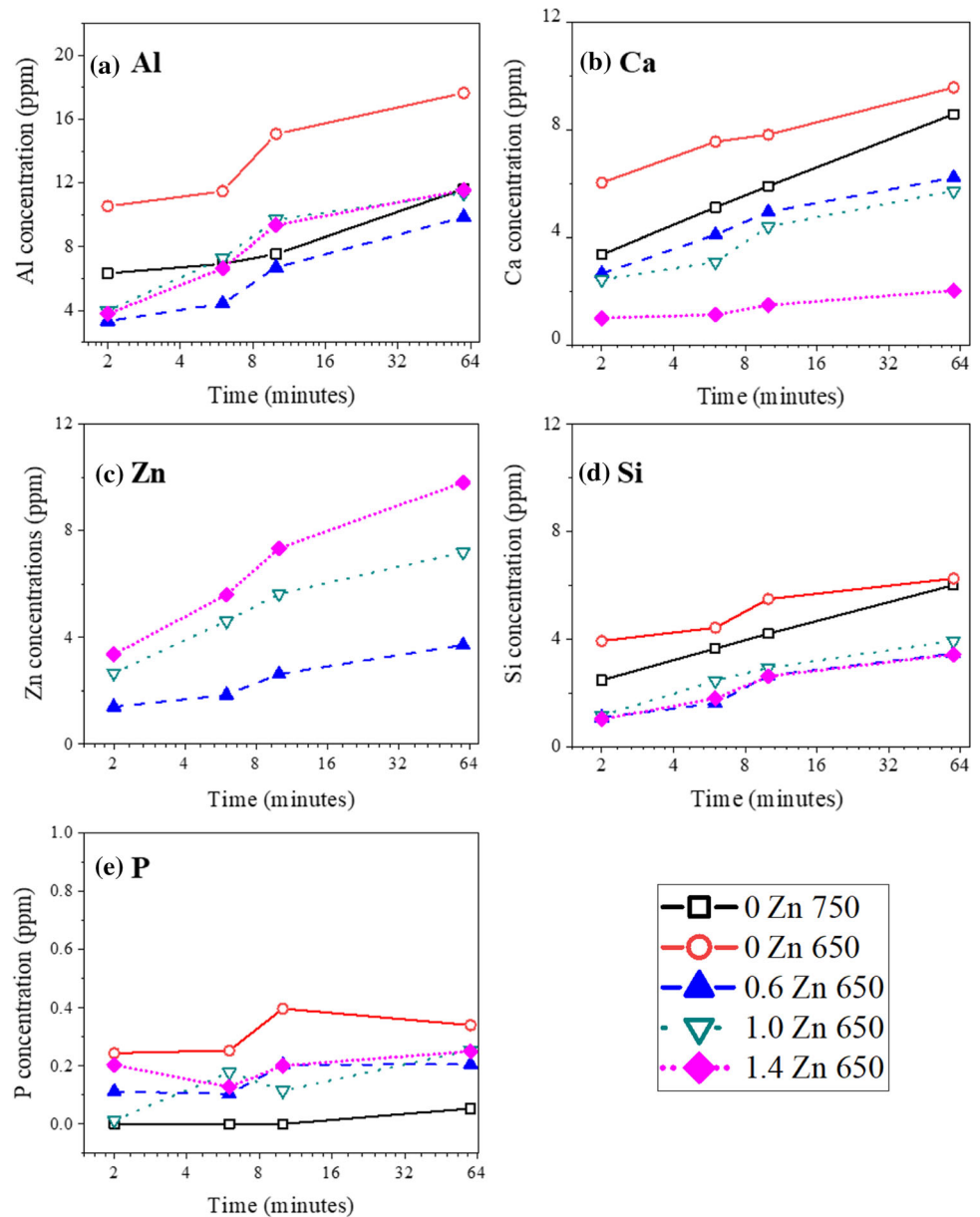


Table 2 ANOVA analysis for the compressive strength for the sol-gel-derived GICs containing different ZnO doping and the calcination temperatures

Source	DF	Seq SS	Adj SS	Adj MS	F	P
Zn	2	1686.88	1686.88	843.44	14.95	0.001
Temperature	1	1195.28	1195.28	1195.28	21.19	0.001
Zn*temperature	2	380.94	380.94	190.47	3.38	0.069
Error	12	676.84	676.84	56.40		
Total	17	3939.94				

of ZnO content (x) of 0.2, 0.6 and 1.0 and calcination temperature at 600°C , 650°C , 700°C and 750°C on the setting time and compressive strength of the sol-gel GICs were studied in the next experiment.

Setting time and compressive strength

The net setting time of the cement paste in Fig. 5 demonstrates that increasing the calcination temperature of the sol-gel glass extended the setting time of

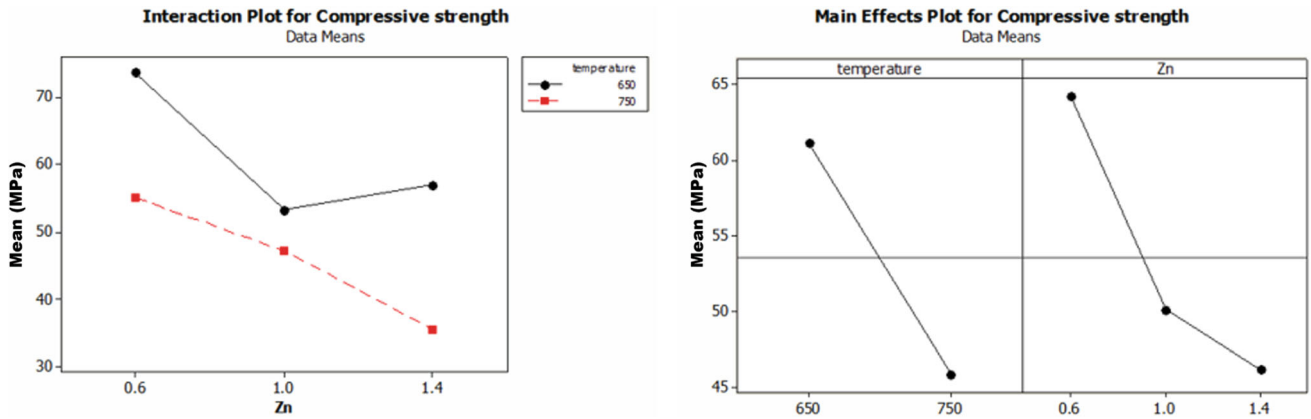


Figure 4 Main effect plot and the interaction plot for compressive strength of the sol-gel-derived GIC containing different ZnO doping and the calcination temperatures.

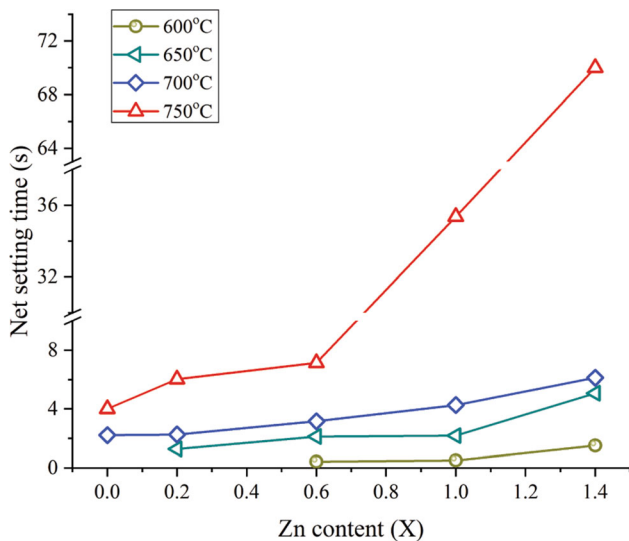


Figure 5 Net setting time of the GIC prepared from the sol-gel ionomer glass belonging to the system of $4.5\text{SiO}_2\text{-}4.0\text{Al}_2\text{O}_3\text{-}0.16\text{P}_2\text{O}_5\text{-}(2-x)\text{Ca-xZnO-}2\text{F}_2$, where $x = 0, 0.2, 0.6, 1.0$ and 1.4 and calcined at 600°C , 650°C , 700°C and 750°C .

GICs. The increasing of ZnO content slightly increased the setting time as well. The cement with low ZnO content and calcined at below 650°C was unable to form because of rapid setting time. Meanwhile, the cement with 1 mol of ZnO calcined at 750°C presented a drastic increase of setting time due to the existence of crystal structure.

The extension of the setting time for the sol-gel GIC can be explained from the glass structural change of the sol-gel glass. According to the structural analysis, the increase of calcination temperature and ZnO content led to an increase in BO structure. This structure was reported that decreased the acid

susceptibility of the glass [15]. Moreover, increasing ZnO content and the calcination temperature reduced the release level of Ca^{2+} ions. Thus, there might have been a lack of ions to crosslink with the polymeric liquid in the setting reaction resulting in the extension of the setting time.

Figure 6 revealed the compressive strength of the sol-gel GIC doped with different ZnO contents and calcination temperatures. At a calcination temperature of 750°C , the compressive strength of the cement decreased as adding of ZnO content in the glass composition. Whereas the calcination

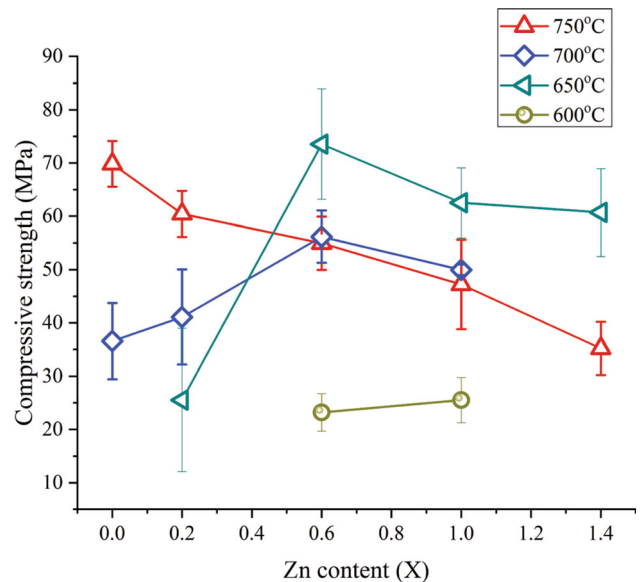


Figure 6 Compressive strength of the sol-gel GIC belonging to the system of $4.5\text{SiO}_2\text{-}4.0\text{Al}_2\text{O}_3\text{-}0.16\text{P}_2\text{O}_5\text{-}(2-x)\text{Ca-xZnO-}2\text{F}_2$, where $x = 0.2, 0.6,$ and 1.0 and calcination temperature of 600°C , 650°C , 700°C and 750°C .

temperature at 700 °C and 650 °C, the cement with 0.6 mol of ZnO exhibited the highest compressive strength as compared in the group of ZnO-doped sol-gel cement. However, below 0.6 mol of ZnO content, the compressive strength was poor because it was difficult to handle and could not be molded for homogeneous samples.

Our results showed that the calcination temperature should be considered when optimizing the setting time and compressive strength of the sol-gel GIC. Since the increase of ZnO content in the sol-gel glass composition can extend the setting time and reduce the strength, the calcination temperature should be compromised to obtain the suitable setting time and the compressive strength.

The mechanical properties of glass ionomer cement could be influenced by various factors, such as glass composition, powder to liquid ratio (P/L), type of the liquid phase, reinforcement, etc. [33–35]. The glass powder in this study was synthesized by the sol-gel method with different glass compositions as compared to the commercial product resulting in significantly different glass structure and ion-releasing behavior. In addition, the type of liquid solution and the powder to liquid ratio were different from the commercial product. The sol-gel ionomer glass was limited with a liquid solution at a P/L ratio of 1 while most commercial GIC was mixing with a liquid solution at a P/L ratio of more than 1. The compressive strength in this study can be further improved by increasing the P/L ratio and modifying the glass structure.

According to the good results of the compressive strength and setting time of the sol-gel GIC sample prepared with 0.6 ZnO calcined at 650 °C, it was evaluated in comparison with 0 and 1.4 ZnO GICs as the substitution of ZnO instead of CaO in the glass structure by using the XAS technique. In addition, the effect of the biological properties for the sol-gel 0, 0.6 and 1.4 ZnO GICs was also investigated.

The local structure of ZnO containing GICs

Figure 7a, b show the absorption spectra of the sol-gel GICs from Ca-XANES and Zn-XANES results, respectively. The position of the main energetic transition edge was the same in all samples. This characteristic indicated a similar structure among both sample groups, but the intensity of the spectra was different. The intensity referred to the number of

O atoms around the core atoms which the high intensity indicated the high amount of O atoms. Figure 7a shows that the increase of ZnO content in GIC increases O atoms around Ca atoms. Figure 7b shows that the increase of ZnO content in GIC reduces O atoms around Zn atoms. The number of O atoms around the core atom was further analyzed by the EXAFS technique as shown in Fig. 8.

After the setting reaction of the sol-gel GICs, the local environment of Ca and Zn atoms in the Zn-doped GIC were determined by EXAFS spectra. Figure 8 shows the spectra in R-space at Ca and Zn K-edge. This study observed the coordination number (CN) of O atoms in the first shell of Ca and Zn atoms. The fitting parameter in Table 3 confirmed the XANES result that the increasing of ZnO content increased the average CN of O atoms around Ca atoms but decreased the CN of O atoms around Zn atoms.

According to the fitting parameter of EXAFS results, the O atoms preferred to bond with the Ca atoms than Zn atoms after the setting reaction. This could be assumed that the O atom from the carboxyl group of PAA preferred to crosslink with Ca atoms than Zn atoms. Therefore, the substitution of ZnO instead of CaO depleted the crosslinking ions for the setting reaction of GIC resulting in reducing compressive strength.

Figure 9 illustrates the proposed glass network structure related to Ca^{2+} ions and Zn^{2+} ions location in the sol-gel glass network structure before and after setting to glass ionomer cement which were analyzed by the XPS and XAS techniques in this study. According to the XPS result, Ca^{2+} ions in the Zn-free ionomer glass existed as a network modifier and formed as CaF_2 . When CaO in the glass composition was substituted by ZnO, Ca^{2+} ions were only found in the form of CaF_2 , and Zn^{2+} ions formed in the tetrahedral site and connected to the glass network as a network former through BO structure. The increase of ZnO in the glass composition to 1.4 mol resulted in an increasing fraction of octahedral structure which also connected to the glass network through BO structure.

After these ionomer glasses were attacked by the acid liquid, the glasses released both Ca^{2+} and Zn^{2+} ions with relative amounts of respective CaO and ZnO content in the glass composition. Consequently, the XAS results showed that these two metal ions could crosslink with the -COO^- a group of PAA with

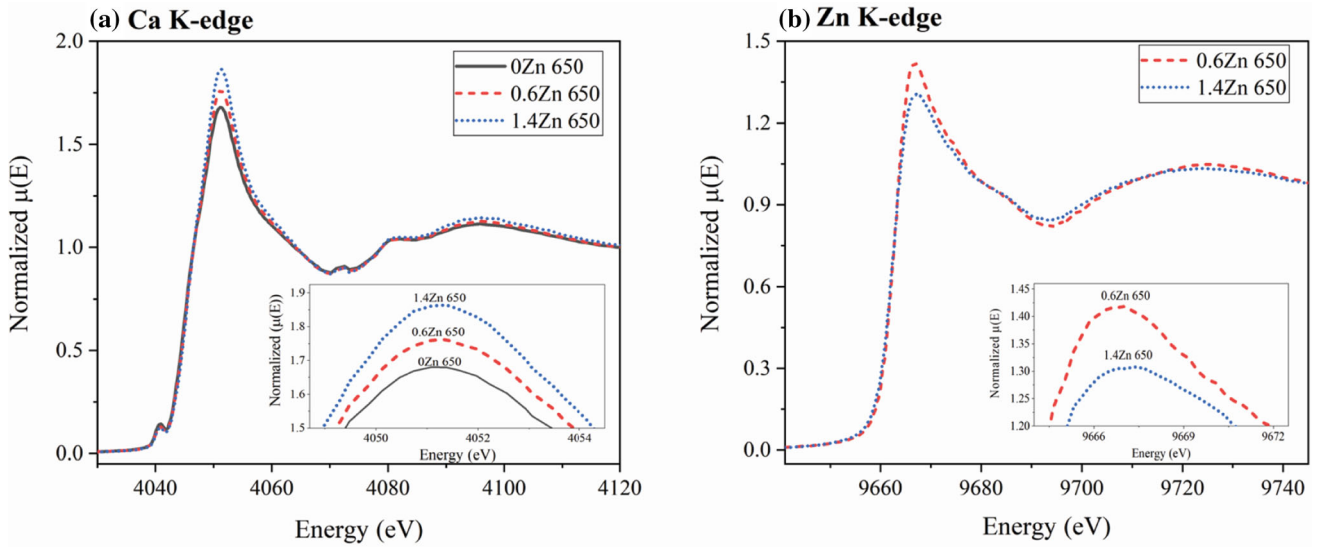


Figure 7 XANES spectra of GIC samples prepared with 0, 0.6 and 1.4 Zn-doped sol-gel glasses calcined at 650 °C at **a** Ca K-edge and **b** Zn K-edge.

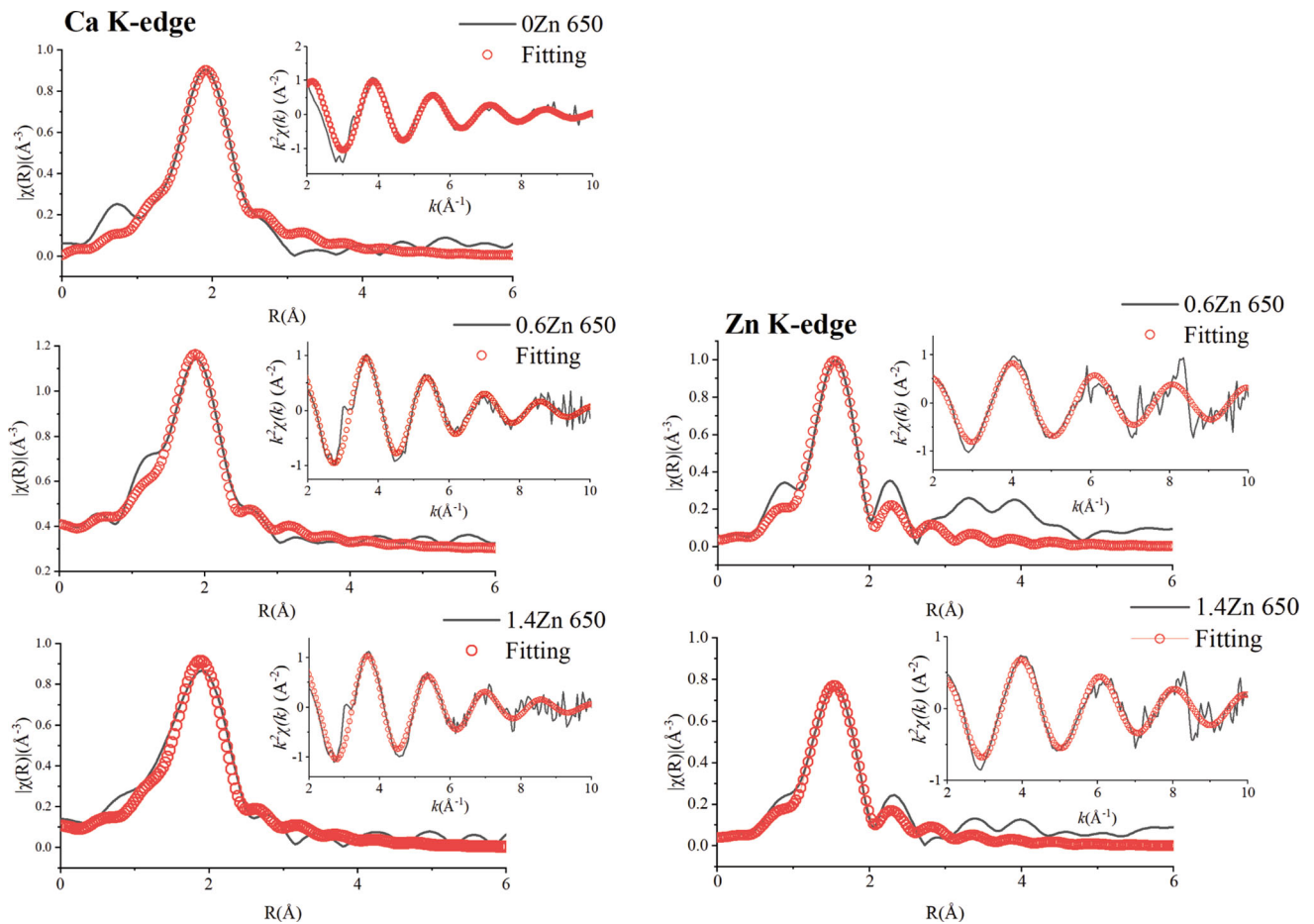


Figure 8 Ca and Zn K-edge EXAFS (weighted by k^2) from the experiment (black line) and fitting (red circle) of GIC samples prepared with 0, 0.6 and 1.4 Zn-doped sol-gel glasses calcined at 650 °C.

Table 3 EXAFT fitting parameters including average coordination number of oxygens around the atom (CN), Debye-Waller factor (σ), interatomic distance (R), and (R -factor)

Sample	Ca K-edge				Zn K-edge			
	CN	σ^2	$R(\text{\AA})$	R -factor	CN	σ^2	$R(\text{\AA})$	R -factor
0Zn	4.326	0.00909	2.380	0.0101	—	—	—	—
0.6Zn	4.746	0.00901	2.382	0.0242	2.092	0.00084	1.993	0.0329
1.4Zn	6.000	0.01068	2.392	0.0257	1.88	0.00265	1.998	0.0198

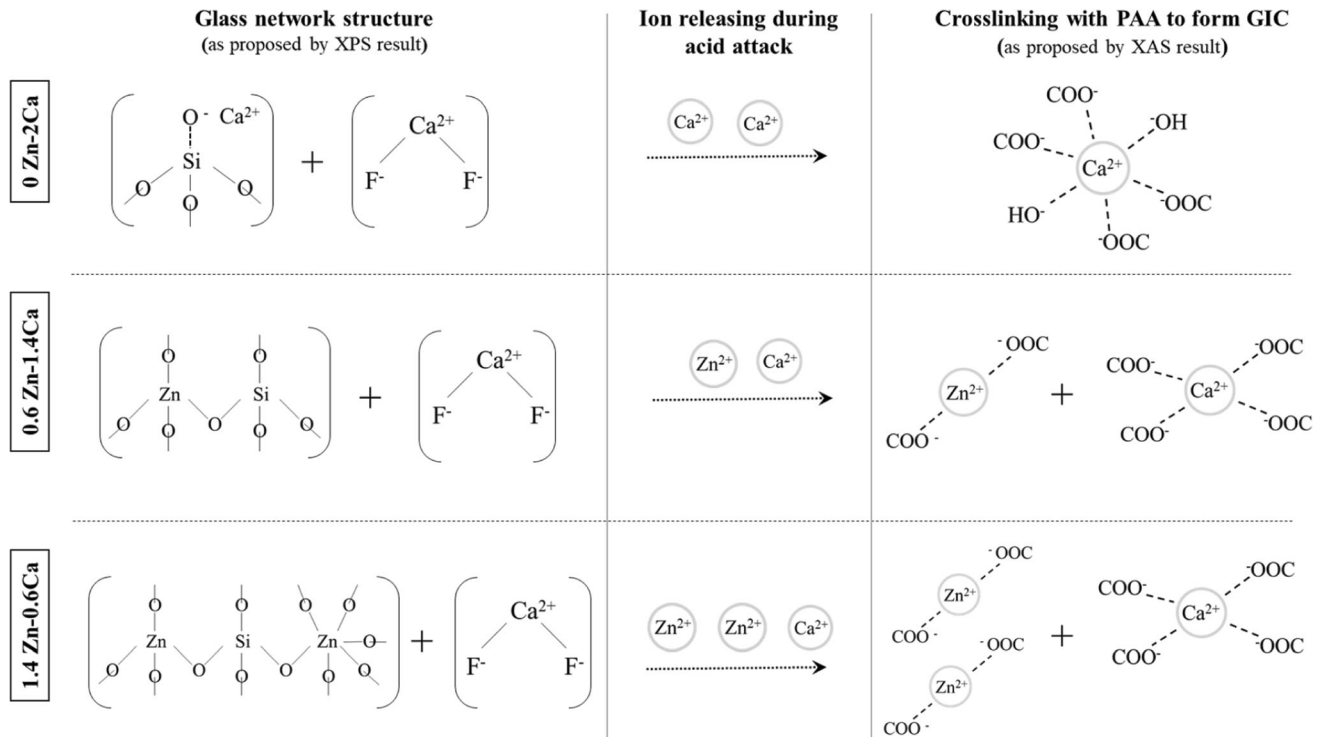


Figure 9 A proposed glass network structure for ZnO instead of CaO in the sol-gel ionomer glass network and form crosslinking with polyacrylic acid in glass ionomer cement after setting.

different coordination complexes. The CN seemed to be determined by many factors i.e., the metal's size, the ligand charge, the charge-donating ability of the ligand and the reaction acidity [36, 37]. The previous study presented that Ca atoms were possibly surrounded by O atoms of carboxylate group with CN in a range of 2–8 [38–40]. The CN of O atoms around Zn atoms was also found in various values in a range of 2–6, where it was compounded with water and bulky organic molecules [41–43]. According to our result, Ca atoms were found to be surrounded by O atoms with CN = 6 for the Zn-free GIC. In the case of CN = 6, Bonapasta reported that 4 of O atoms of the PAA chains placed at the square bases of the octahedron and O atoms of the OH^- ions occupy the two vertices of the octahedron [38]. The substitution of ZnO for CaO resulted in the changing of CN around

Ca atoms from 6 to 4, and Zn atoms were surrounded by O atoms with the CN = 2. Therefore, increasing ZnO content in the ionomer glass reduced the crosslinking for setting reaction of GIC resulting in the reduction of compressive strength.

Antibacterial property

Figure 10 demonstrates the antibacterial activity of the GIC samples with various concentrations of ZnO (0, 0.6 and 1.4 Zn) doped ionomer glass against *S. mutan* under light and dark conditions. In a dark condition, external light exposure was prevented by keeping it in the black box during the incubation period. The result presented that there was no inhibition zone occurring in the sol-gel GIC samples for the dark condition. Interestingly, the ZnO-doped GIC

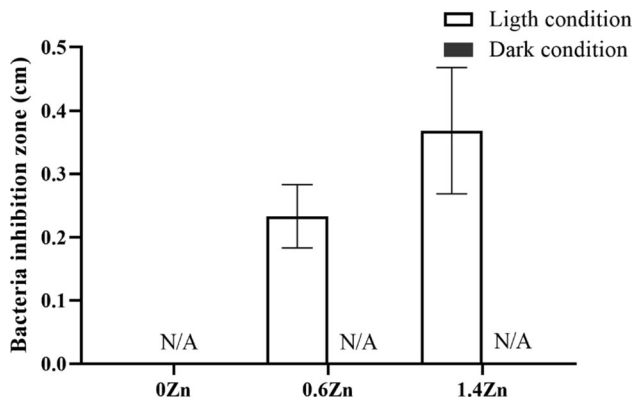


Figure 10 The diameter of inhibition zone against *S. mutans* of the GIC samples prepared with 0, 0.6 and 1.4 Zn-doped sol-gel glasses calcined at 650°C.

presented the inhibition zone around the sample under the light condition, and the inhibition zone was extended with the addition of the amount of ZnO in the glass composition.

The inhibition zone of all Zn-doped incubating under light conditions was greater than 0.1 cm and increased with increasing ZnO content as compared to Zn-free GIC. This was considered to have an antibacterial effect according to the standard SNV 195,920-199 [44]. The antibacterial activity of ZnO was regulated through three mechanisms: photochemical reaction, direct contraction of ZnO particles to the bacteria cell wall, and the release of bactericidal Zn^{2+} ions [45, 46]. Our data showed that the antibacterial activity of ZnO-doped GIC was only activated under light condition; thus, this effect was attributed to the photochemical reaction. The photochemical reaction was described as a photo-induced oxidation process in that ZnO could absorb UV light and generate ROS species such as hydrogen peroxide (H_2O_2) and superoxide ions (O^{2-}). These ROS species were able to penetrate the cells, then inhibit or kill microorganisms [46].

Cell viability

Figure 11a shows the cell viability of NIH/3T3 fibroblast cells after treatment with extracts of the sol-gel GIC with the variation of ZnO contents in glass for 24 h. The MTS assay showed that cell viability of NIH/3T3 fibroblast cells was decreased after treatment with the ZnO-doped sol-gel GICs at 0.6ZnO and 1.4ZnO whereas less cytotoxicity was found for the sol-gel GIC without ZnO doping. With diluting of

the extract concentration to 1:2 and 1:4, cell viability for all samples trended to continuously increase.

Zn^{2+} ions seemed to have disadvantages in terms of biocompatibility. Brauer et al. demonstrated that the possible reason for cytotoxicity was a large amount of Zn^{2+} ions release [47]. Several studies reported that the cytotoxicity of Zn^{2+} ions associated with the production of ROS species which was the same mechanism with the antibacterial effect [48, 49]. However, the dilution of Zn^{2+} ions concentration seemed to reduce the toxicity and have a benefit to cell growth [47].

The previous study reported that the optimum concentration of Zn^{2+} ions on cell toxicity was 350 μM [47]. According to our result, 523 μM of Zn^{2+} ions was released from the sol-gel GIC prepared with 0.6ZnO calcined at 650 °C, as shown in Fig. 11b. This concentration was higher than 350 μM which could be the reason for an adverse effect on the cell viability. After dilution (1:2) of the extracted, the concentration of Zn^{2+} ions might reduce to around 260 μM which drastically increased the cell viability. This improvement of the cell viability was possible to be a benefit in clinical use. It was because the concentration of Zn^{2+} released from the GIC was diluted by the fluid circulation in the oral environment.

Apatite-like formation and tooth-GIC interface

Figure 12 shows the SEM images and EDS results of the sol-gel GIC surfaces after soaking in the DI water and artificial saliva for 5 days. The apatite-like layer occurred on all GIC surfaces after soaking in artificial saliva, and the thickness of the apatite-like layer was greater when ZnO content increased. Meanwhile, there was no apatite-like layer on all GIC surfaces soaking in DI water. The apatite-like layer could be confirmed by EDS results that the ratio of Ca/P should be in the range of 1.30–1.67 [50]. Our result presented that the Ca/P ratio was around 1.40 where ZnO was substituted for CaO in the ionomer glass composition. This could be indicated that there was an apatite-like layer on the GIC surfaces for artificial saliva immersion.

The formation of the apatite layer was associated with the deposition of calcium and phosphate on the cement surface, then precipitated into an apatite-like crystal lattice [51]. This apatite layer was reported to enhance a chemical bond between GIC and tooth

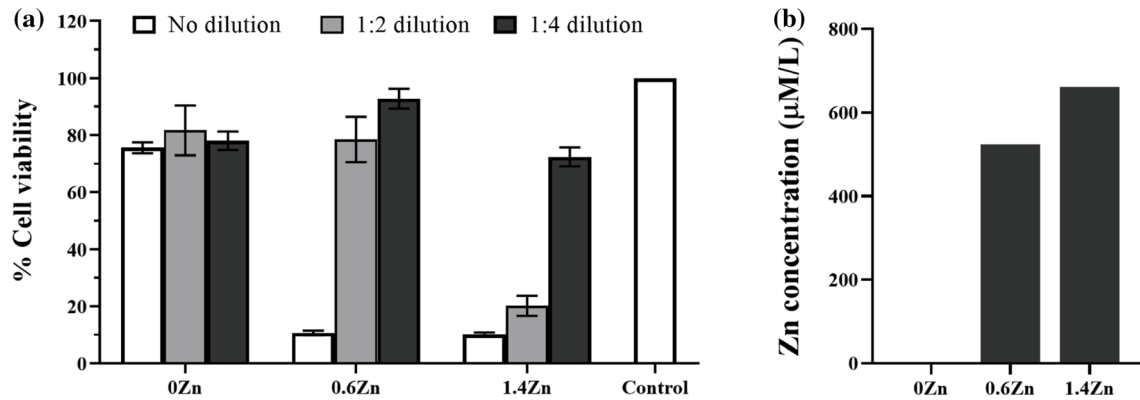


Figure 11 Effect of Zn content in the sol-gel GIC on the NIH/3T3 cell viability (indirect contact). **a** %cell viability treated with different concentrations of the extracted solutions. The cells with fresh culture medium was used as a negative control. Values were

expressed as the mean \pm standard error of the mean of three independent experiments and **b** the Zn²⁺ ion-releasing concentration in the as-received extracted solutions analyzed by the ICP-OES technique.

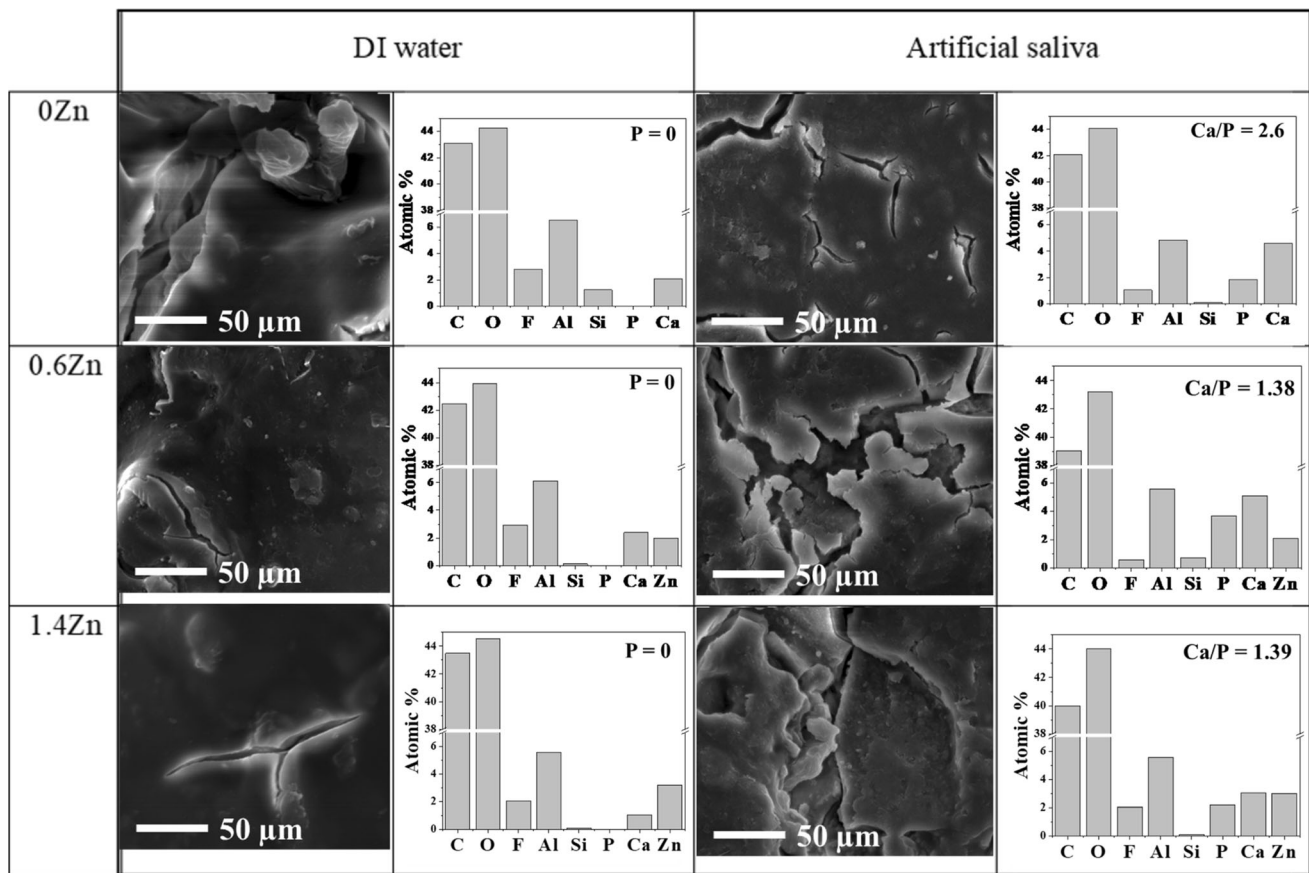


Figure 12 SEM micrographs of GIC surface for the sol-gel GIC prepared with the sol-gel glasses doped different ZnO contents and calcined at 650 °C after soaking in DI water and artificial saliva for 5 days, respectively (magnification \times 5000).

structure [52]. Therefore, the ability of apatite-like formation on the GIC surface after soaking in saliva solution could indicate the potential for having a high level of bioactivity.

Figure 13 illustrates the interfacial area between the tooth and the sol-gel GIC with and without ZnO contents, observed by the SEM technique, to determine the probability of the success and failure of the

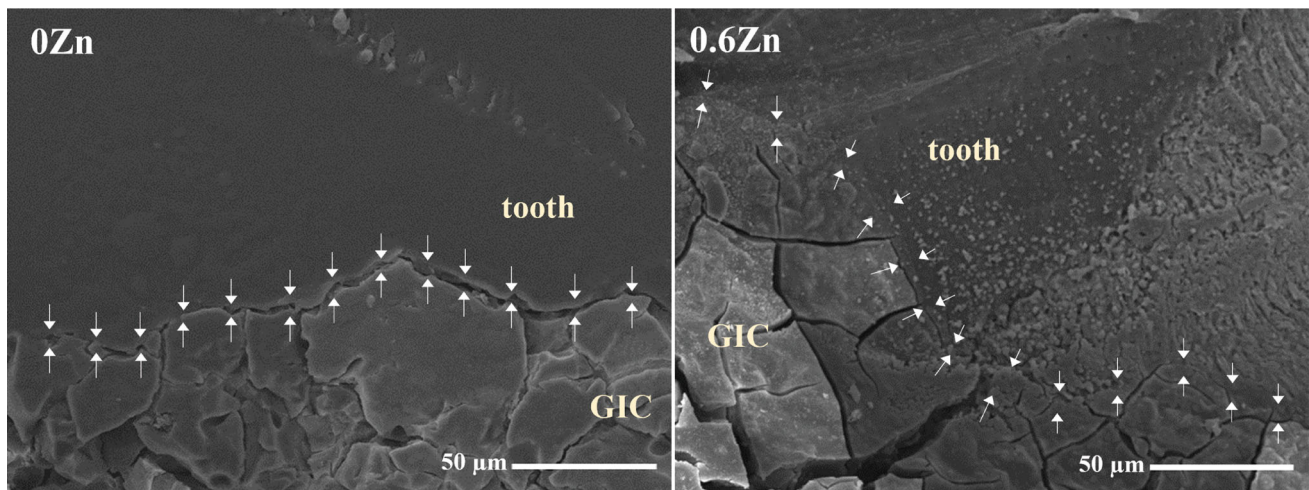


Figure 13 SEM images of the interfacial area between the tooth and the sol-gel GIC samples prepared with 0.6 ZnO-doped glass and calcined at 650 °C as compared to ZnO free GIC.

restoration. The result showed a detachment between Zn-free GIC and the tooth, while ZnO-doped GIC showed complete adaptation to the tooth. This detachment between GIC and tooth structure could happen because of drying the specimens for SEM evaluation. The main mechanism of GIC bonding with tooth structure is based on the ionic reaction of the carboxyl group with calcium and phosphate on the tooth surface. However, this result demonstrated that the presence of zinc in the glass structure could promote the sealing of the tooth surface. Moreover, the previous work reported that zinc potentially stimulates hard-tissue mineralization by interaction with the phosphate in the tooth structure [51]. This interaction might enhance the bonding response between the tooth and the GIC.

The manufacturers recently introduced zinc containing GIC, i.e., CAREDYNE RESTORE from GC Japan and ChemFil™ Rock from Dentsply USA. CAREDYNE RESTORE is a new GIC product composing of “BioUnion Filler”, which releases fluoride, zinc and calcium ions. The releasing level of zinc from this product was reported to reach the level to inhibit biofilm formation [53]. This product also shows a high remineralization performance, appropriate for the prevention and restoration of root caries [54, 55]. For the ChemFil™ Rock, it is a new type of GIC with an enhanced setting reaction by the presence of zinc in glass composition. The presence of zinc increased durability and able to use in stress-bearing situations along with posterior tooth restoration [6]. These commercial products showed

the benefit of zinc containing GIC for dental restorative materials. This study also demonstrated the substitute of zinc for calcium site in glass composition synthesized by the sol-gel method at low temperature, which improved both of biological and antibacterial characteristics of the glass ionomer cement.

Conclusions

ZnO doping instead of CaO in the glass composition and the calcination temperature for the glass synthesized by the sol-gel method was studied in this work. The result showed that ZnO was unable to replace the CaO in the sol-gel ionomer glass. The increasing of ZnO content and calcination temperature induced the crystal structure of ZnAl_2O_4 and ZnO_2 . After the setting reaction, the EXAFS data revealed that O atoms from the $-\text{COO}^-$ functional group of PAA liquid preferred to bond with Ca^{2+} ions than Zn^{2+} ions. Thus, the compressive strength of the ZnO-doped GIC decreased with the increase of ZnO content. However, the compressive strength could be maintained by decreasing the calcination temperature. This study presented that the sol-gel GIC prepared with 0.6Zn glass calcined at 650 °C had the most promising result in terms of setting time and compressive strength.

Interestingly, the antibacterial effect of ZnO content in glass composition was excellent under the light condition as the photocatalysis effect. Additionally,

the GIC prepared with the 0.6ZnO glass presented slightly toxic to cells. This could be improved in further study by reducing the amount of ZnO in the glass composition. Furthermore, the sol-gel GIC with ZnO doping also improved bioactivity and tooth adhesion.

Acknowledgements

The authors would like to thank the Synchrotron Light Research Institute (Public Organization), Thailand for the XPS (BL5.3) and XAS (BL5.2) facilities. Thanks to Mr Chinawat Ekwongsa for helping in XANES and EXAFT data analysis.

Funding

This paper was financially supported by the Royal Golden Jubilee (RGJ) PhD Program from Thailand Research Fund (PHD/0058/2558) and Suranaree University of Technology.

Declarations

Conflict of interest The authors have no conflicts of interest to declare that are relevant to the content of this article.

References

- Wong A, Subar PE, Young DA (2017) Dental caries: an update on dental trends and therapy. *Adv Pediatr* 64:307–330. <https://doi.org/10.1016/j.yapd.2017.03.011>
- California DB (2005) The fact about filling. Department of consumer affairs, Carlifornia
- Sidhu SK, Nicholson JW (2016) A review of glass-ionomer cements for clinical dentistry. *J Funct Biomater* 7:16. <https://doi.org/10.3390/jfb7030016>
- Li Y, Zhang W, Niu J, Chen Y (2012) Mechanism of photogenerated reactive oxygen species and correlation with the antibacterial properties of engineered metal-oxide nanoparticles. *ACS Nano* 6:5164–5173. <https://doi.org/10.1021/nm300934k>
- Tiama T, Abd N, Tohamy K, Soliman I (2017) In vitro bioactivity and antibacterial activity of zn and sr containing glass ionomer cement prepared by a quick alkali-mediated sol-gel method. *EC Dent Sci* 4:136–146
- Patil K, Patel A, Kunte S, Shah P, Kaur B, Paranna S (2020) Comparative evaluation of the mechanical properties of zinc-reinforced glass ionomer cement and glass ionomer type IX cement: an in vitro study. *Int J Clin Pediatr Dent* 13:381–389. <https://doi.org/10.5005/jp-journals-10005-1798>
- Kumar A, Raj A, Singh D, Donthagani S, Kumar M, Ramesh K (2021) A new zinc reinforced glass ionomer cement: a boon in dentistry. *J Pharm Bioallied Sci* 13:272–275. https://doi.org/10.4103/jpbs.JPBS_730_20
- Thongsri O, Srisuwan S, Thaitalay P, Dangwiriyaikul R, Aengchuan P, Chanlek N, Talabnin C, Suksaweang S, Rattanachan ST (2021) Influence of Al₂O₃ and P₂O₅ contents in sol-gel ionomer glass system on the structure and their cement properties. *J Sol-Gel Sci Technol* 98:441–451. <https://doi.org/10.1007/s10971-021-05519-9>
- Zhang S, Stamboulis A (2016) Effect of zinc substitution for calcium on the crystallisation of calcium fluoro-aluminosilicate glasses. *J Non Cryst Solids* 432:300–306. <https://doi.org/10.1016/j.jnoncrysol.2015.10.025>
- Kusumoto H (2009) Characterisation of Mg, Sr, and Zn containing fluoro-aluminosilicate glasses and their glass polyalkenoate cements. PhD Dissertation, Imperial College, London
- Bertolini MJ, Zaghete MA, Gimenes R (2005) Development of an experimental glass ionomer cement containing niobium and fluoride. *J Non Cryst Solids* 351:3884–3887. <https://doi.org/10.1016/j.jnoncrysol.2005.10.008>
- Kajihara K (2013) Recent advances in sol-gel synthesis of monolithic silica and silica-based glasses. *J Asian Ceram Soc* 1:121–133. <https://doi.org/10.1016/j.jascer.2013.04.002>
- Mukherjee SP (1980) Sol-gel processes in glass science and technology. *J Non Cryst Solids* 42:477–488. [https://doi.org/10.1016/0022-3093\(80\)90046-0](https://doi.org/10.1016/0022-3093(80)90046-0)
- Roy B, Jain H, Saha SK, Chakravorty D (1995) Comparison of structure of alkali silicate glasses prepared by sol-gel and melt-quench methods. *J Non Cryst Solids* 183:268–276. [https://doi.org/10.1016/0022-3093\(94\)00633-4](https://doi.org/10.1016/0022-3093(94)00633-4)
- Wren A, Clarkin O, Laffir F, Ohtsuki C, Kim IY, Towler M (2009) The effect of glass synthesis route on mechanical and physical properties of resultant glass ionomer cements. *J Mater Sci Mater Med* 20:1991–1999. <https://doi.org/10.1007/s10856-009-3781-6>
- Tang V, Otto K, Seering W (2014) Using design of experiments (DOE) for decision analysis. Paper presented at the International Conference on Engineering Design, ICED'07 Cite des sciences et de l'industrie, Paris, France, 01/23
- Kidkhunthod P (2017) Structural studies of advanced functional materials by synchrotron-based x-ray absorption spectroscopy: BL5.2 at SLRI, Thailand. *Adv Nat Sci*

- Nanosci 8:035007. <https://doi.org/10.1088/2043-6254/aa7240>
- [18] Neville M (2001) IFEFFIT : interactive XAFS analysis and FEFF fitting. *J Synchrotron Radiat* 8:322–324. <https://doi.org/10.1107/S0909049500016964>
- [19] Jain A, Ong SP, Hautier G, Chen W, Richards WD, Dacek S, Cholia S, Gunter D, Skinner D, Ceder G, Persson KA (2013) Commentary: the Materials Project: a materials genome approach to accelerating materials innovation. *APL Mater* 1:011002. <https://doi.org/10.1063/1.4812323>
- [20] Paiva L, Fidalgo TKS, da Costa LP, Maia LC, Balan L, Anselme K, Ploux L, Thiré RMSM (2018) Antibacterial properties and compressive strength of new one-step preparation silver nanoparticles in glass ionomer cements (NanoAg-GIC). *J Dent* 69:102–109. <https://doi.org/10.1016/j.jdent.2017.12.003>
- [21] Kamalak H, Kamalak A, Taghizadehghalehjoughi A, Hacımüftüoğlu A, Nalçı KA (2018) Cytotoxic and biological effects of bulk fill composites on rat cortical neuron cells. *Odontology* 106:377–388. <https://doi.org/10.1007/s10266-018-0354-5>
- [22] El Mallakh BF, Sarkar NK (1990) Fluoride release from glass-ionomer cements in de-ionized water and artificial saliva. *Dent Mater* 6:118–122. [https://doi.org/10.1016/S0109-5641\(05\)80041-7](https://doi.org/10.1016/S0109-5641(05)80041-7)
- [23] Bogomolova LD, Pavlushkina TK, Morozova IV (2006) Formation of glass synthesized by sol-gel technology. *Glass Ceram* 63:254–258. <https://doi.org/10.1007/s10717-006-0092-y>
- [24] Zanutto ED (1992) The formation of unusual glasses by sol-gel processing. *J Non Cryst Solids* 147–148:820–823. [https://doi.org/10.1016/S0022-3093\(05\)80723-9](https://doi.org/10.1016/S0022-3093(05)80723-9)
- [25] Tshabalala KG, Cho SH, Park JK, Pitale SS, Nagpure IM, Kroon RE, Swart HC, Ntwaeaborwa OM (2011) Luminescent properties and X-ray photoelectron spectroscopy study of ZnAl₂O₄:Ce³⁺, Tb³⁺ phosphor. *J Alloys Compd* 509:10115–10120. <https://doi.org/10.1016/j.jallcom.2011.08.054>
- [26] Stranick MA, Root MJ (1991) Influence of strontium on monofluorophosphate uptake by hydroxyapatite XPS characterization of the hydroxyapatite surface. *Colloids Surf* 55:137–147. [https://doi.org/10.1016/0166-6622\(91\)80088-6](https://doi.org/10.1016/0166-6622(91)80088-6)
- [27] Bezerra CdS, Valerio MEG (2016) Structural and optical study of CaF₂ nanoparticles produced by a microwave-assisted hydrothermal method. *Physica B Condens Matter* 501:106–112. <https://doi.org/10.1016/j.physb.2016.08.025>
- [28] Zhang D, Qingjie G, Ren Y, Wang C, Shi Q, Wang Q, Xiao X, Wang W, Fan Q (2017) Influence of inversion defects and Cr–Cr pairs on the photoluminescent performance of ZnAl₂O₄ crystals. *J Sol-Gel Sci Technol* 85:121–131. <https://doi.org/10.1007/s10971-017-4527-4>
- [29] Bernasconi A, Dapiaggi M, Pavese A, Agostini G, Bernasconi M, Bowron DT (2016) Modeling the structure of complex aluminosilicate glasses: the effect of zinc addition. *J Phys Chem B* 120:2526–2537. <https://doi.org/10.1021/acs.jpcc.5b10886>
- [30] Nicholson JW, Coleman NJ, Sidhu SK (2021) Kinetics of ion release from a conventional glass-ionomer cement. *J Mater Sci Mater Med* 32:1–10. <https://doi.org/10.1007/s10856-021-06501-1>
- [31] Kunle A, Nicholson John W (2014) A study of phosphate ion release from glass-ionomer dental cements. *Ceram-Silik* 58:210–214
- [32] Nicholson JW (2018) Maturation processes in glass-ionomer dental cements. *Acta Biomater Odontol Scand* 4:63–71. <https://doi.org/10.1080/23337931.2018.1497492>
- [33] Alhalawani AMF, Curran DJ, Boyd D, Towler MR (2016) The role of poly(acrylic acid) in conventional glass polyalkenoate cements. *J Polym Eng* 36:221–237. <https://doi.org/10.1515/polyeng-2015-0079>
- [34] Baig MS, Fleming GJP (2015) Conventional glass-ionomer materials: a review of the developments in glass powder, polyacid liquid and the strategies of reinforcement. *J Dent* 43:897–912. <https://doi.org/10.1016/j.jdent.2015.04.004>
- [35] Fleming G, Farooq A, Barralet J (2003) Influence of powder/liquid mixing ratio on the performance of a restorative glass-ionomer dental cement. *Biomaterials* 24:4173–4179. [https://doi.org/10.1016/S0142-9612\(03\)00301-6](https://doi.org/10.1016/S0142-9612(03)00301-6)
- [36] Dudev M, Wang J, Dudev T, Lim C (2006) Factors governing the metal coordination number in metal complexes from cambridge structural database analyses. *J Phys Chem B* 110:1889–1895. <https://doi.org/10.1021/jp054975n>
- [37] Pan HB, Darvell BW (2007) Solubility of calcium fluoride and fluorapatite by solid titration. *Arch Oral Biol* 52:861–868. <https://doi.org/10.1016/j.archoralbio.2007.03.002>
- [38] Bonapasta AA, Buda F, Colombet P (2001) Interaction between Ca ions and poly(acrylic acid) chains in macrodefect-free cements: a theoretical study. *Chem Mater* 13:64–70. <https://doi.org/10.1021/cm000505o>
- [39] Katz AK, Glusker JP, Beebe SA, Bock CW (1996) Calcium ion coordination: a comparison with that of beryllium, magnesium, and zinc. *J Am Chem Soc* 118:5752–5763. <https://doi.org/10.1021/ja953943i>
- [40] Vao-soongnern V, Merat K, Horpibulsuk S (2015) Interaction of the calcium ion with poly(acrylic acid) as investigated by a combination of molecular dynamics simulation and X-ray absorption spectroscopy. *J Polym Res* 23:7. <https://doi.org/10.1007/s10965-015-0895-z>

- [41] Daley T, Opuni KB, Raj E, Dent AJ, Cibin G, Hyde TI, Sankar G (2021) Monitoring the process of formation of ZnO from ZnO₂ using in situ combined XRD/XAS technique. *J Condens Matter Phys* 33:264002. <https://doi.org/10.1088/1361-648x/abfb91>
- [42] Thomas SA, Mishra B, Myneni SCB (2019) High energy resolution-X-ray absorption near edge structure spectroscopy reveals Zn ligation in whole cell bacteria. *J Phys Chem Lett* 10:2585–2592. <https://doi.org/10.1021/acs.jpclett.9b01186>
- [43] Krężel A, Maret W (2016) The biological inorganic chemistry of zinc ions. *Arch Biochem Biophys* 611:3–19. <https://doi.org/10.1016/j.abb.2016.04.010>
- [44] Schuhlraden K, Stich L, Schmidt J, Steinkasserer A, Boccaccini AR, Zinser E (2020) Cu, Zn doped borate bioactive glasses: antibacterial efficacy and dose-dependent in vitro modulation of murine dendritic cells. *Biomater Sci* 8:2143–2155. <https://doi.org/10.1039/C9BM01691K>
- [45] Joe A, Park S-H, Shim K-D, Kim D-J, Jhee K-H, Lee H-W, Heo C-H, Kim H-M, Jang E-S (2017) Antibacterial mechanism of ZnO nanoparticles under dark conditions. *J Ind Eng Chem* 45:430–439. <https://doi.org/10.1016/j.jiec.2016.10.013>
- [46] Sirelkhatim A, Mahmud S, Seeni A, Kaus NHM, Ann LC, Bakhori SKM, Hasan H, Mohamad D (2015) Review on zinc oxide nanoparticles: antibacterial activity and toxicity mechanism. *Nanomicro Lett* 7:219–242. <https://doi.org/10.1007/s40820-015-0040-x>
- [47] Brauer DS, Gentleman E, Farrar DF, Stevens MM, Hill RG (2011) Benefits and drawbacks of zinc in glass ionomer bone cements. *Biomed Mater* 6:045007. <https://doi.org/10.1088/1748-6041/6/4/045007>
- [48] Patrón-Romero L, Luque PA, Soto-Robles CA, Nava O, Vilchis-Nestor AR, Barajas-Carrillo VW, Martínez-Ramírez CE, Chávez Méndez JR, Alvelais Palacios JA, Leal Ávila MÁ, Almanza-Reyes H (2020) Synthesis, characterization and cytotoxicity of zinc oxide nanoparticles by green synthesis method. *J Drug Deliv Sci Technol* 60:101925. <https://doi.org/10.1016/j.jddst.2020.101925>
- [49] Saber M, Hayaei-Tehrani R-S, Mokhtari S, Hoorzad P, Esfandiari F (2021) In vitro cytotoxicity of zinc oxide nanoparticles in mouse ovarian germ cells. *Toxicol Vitro* 70:105032. <https://doi.org/10.1016/j.tiv.2020.105032>
- [50] Drouet C (2013) Apatite formation: why it may not work as planned, and how to conclusively identify apatite compounds. *BioMed Res Int* 2013:490946. <https://doi.org/10.1155/2013/490946>
- [51] Lynch R (2011) Zinc in the mouth, its interactions with dental enamel and possible effects on caries; a review of the literature. *Int Dent J* 61(Suppl 3):46–54. <https://doi.org/10.1111/j.1875-595X.2011.00049.x>
- [52] Chen S, Cai Y, Engqvist H, Xia W (2016) Enhanced bioactivity of glass ionomer cement by incorporating calcium silicates. *Biomater* 6:e1123842. <https://doi.org/10.1080/021592535.2015.1123842>
- [53] Kohno T, Tsuboi R, Kitagawa H, Imazato S (2019) Zinc-Ion release and recharge ability of gic containing biounion filler. In: Paper presented at the 2019 IADR/AADR/CADR general session, Vancouver, BC, Canada
- [54] Kaga N, Nagano-Takebe F, Nezu T, Matsuura T, Endo K, Kaga M (2020) Protective effects of GIC and S-PRG filler restoratives on demineralization of bovine enamel in lactic acid solution. *Materials* 13:2140. <https://doi.org/10.3390/ma13092140>
- [55] Nagano Y, Mori D, Kumagaia T (2019) Evaluation of carelyne restore on shear-bond strength and remineralization. In: Paper presented at the the third biennial meeting of the international academy of adhesive dentistry, the Palazzo della Cultura e dei Congressi, Bologna, Italy

Publisher's Note Springer Nature remains neutral with regard to jurisdictional claims in published maps and institutional affiliations.